J. Fluid Mech., page 1 of 28
doi:10.1017/jfm.2011.54

Analysis of mechanisms for platelet near-wall excess under arterial blood flow conditions

L. CROWL[1]† AND A. L. FOGELSON[2]

[1]Department of Mathematics, University of Utah, 155 South 1400 East, Salt Lake City, UT 84112, USA

[2]Department of Mathematics and Department of Bioengineering, 155 South 1400 East, University of Utah, Salt Lake City, UT 84112, USA

(Received 18 February 2010; revised 20 January 2011; accepted 31 January 2011)

The concentration of platelets near the blood vessel wall is important because platelets survey the condition of the vessel wall and respond to injuries to it. Under arterial flow conditions, platelets are non-uniformly distributed across the vessel lumen and have a high concentration within a few microns of the vessel wall. This is believed to be a consequence of the complex motion of red blood cells which constitute a large fraction of the blood's volume. We use a novel lattice Boltzmann-immersed boundary method to simulate, in two dimensions, the motion of dense red blood cell suspensions and their effect on platelet-sized particles. We track the development of a red blood cell-free layer near the wall and the later development of the platelet near-wall excess. We find that the latter develops more quickly at high wall shear rates and that the magnitude of the excess and its proximity to the wall are dependent on haematocrit. Treating the simulation data as if it were generated by a drift–diffusion process, we find that the effective lateral platelet diffusivity depends strongly on lateral position; it has a magnitude of order of $10^{-6}\,\mathrm{cm}^2\,\mathrm{s}^{-1}$ over much of the lumen but drops to almost zero close to the wall. This large effective diffusivity over the core of the lumen combined with reduced space for platelets in this region because of the inward migration of red blood cells largely but not completely accounts for the observed platelet-concentration profiles. We present evidence for a highly localized red blood cell-induced platelet drift at the edge of the red cell-free layer and suggest a physical mechanism that may generate it.

Key words: blood flow, capsule/cell dynamics, suspensions

1. Introduction

Platelets are small, rigid cells that circulate in the bloodstream and play a prominent role in blood clotting in the event of an injury to the vascular wall. Under arterial and arteriolar flow conditions, platelets are highly concentrated near blood vessel walls, positioning them very well to respond if the vessel wall is damaged. This enhanced near-wall concentration has been demonstrated *in vivo* using intravital fluorescent microscopy (see Tangelder *et al.* 1985; Woldhuis *et al.* 1992), and *in vitro* using platelet-sized latex beads in flowing red blood cell (RBC) suspensions (see Tilles & Eckstein 1987; Eckstein, Tilles & Millero 1988). Using the results of platelet adhesion experiments, Turitto, Benis & Leonard (1972) discovered that platelets in

† Email address for correspondence: crowl@math.utah.edu

flowing whole blood experience a complex motion roughly characterized as 'enhanced diffusion'.

To better determine which factors affect the cross-sectional distribution of platelets in flowing blood, Tilles & Eckstein (1987) performed a series of experiments in a $50\,\mu m \times 1000\,\mu m$ rectangular channel. Suspensions of red cell ghosts and fluorescent platelet-size latex beads (diameter $2.38\,\mu m$) were perfused through the channel at a constant flow rate controlled by a syringe pump. The shear rates studied were in the range of 50–3180 s^{-1} with haematocrits (volume fraction of RBCs) ranging from 7 % to 45 %. Eckstein fit his experimental results with a phenomenological 'drift–diffusion' model involving a net drift of beads towards the flow chamber walls that balances the enhanced diffusion of beads to produce the observed concentration profiles (see Eckstein & Belgacem 1991; Yeh, Calvez & Eckstein 1994). The shortcoming of this drift–diffusion formulation is that it only reproduces experimental conditions, and so no extrapolation beyond experimental results can be made concerning platelet dynamics.

Recently, Crowl & Fogelson (2010) presented a two-dimensional computational model for flowing whole blood that accurately represents RBCs and platelets. In that paper, it was shown that the model reproduces the platelet near-wall excess concentration seen experimentally. It was also shown that the time scale on which the near-wall excess develops is about 500 ms at a shear rate of $1100\,s^{-1}$. In the present paper, we use this model to characterize how the RBCs and platelet dynamics depend on the shear rate, haematocrit and platelet size. By analysing data produced in computational experiments using the model, we extract effective RBC and platelet-diffusion coefficients and determine their variation with position across the vessel lumen and their dependence on the shear rate. The detailed simulation data further allow us to identify specific physical mechanisms behind the development of the platelet near-wall excess.

A number of numerical methods for modelling large numbers of RBCs have been developed in recent years. Bagchi (2007) studied the dynamics of the blood flow in microvessels using a two-dimensional (2D) immersed boundary method with individual deformable RBC liquid capsules. MacMeccan *et al.* (2009) developed a three-dimensional (3D) coupled lattice Boltzmann-finite element method to study the behaviour of dense suspensions of deformable particles. Dupin *et al.* (2007) simulated 3D deformable particles including RBCs at low shear rates of $10\,s^{-1}$ using a lattice Boltzmann method with Lagrangian deformable particles. To our knowledge, these 3D simulations are limited to low shear rates and short times that are not appropriate for studying the development of high platelet concentrations near the vessel walls and the motions that lead to it.

2. Lattice Boltzmann-immersed boundary method

Using the lattice Boltzmann-immersed boundary method described in our earlier paper (see Crowl & Fogelson 2010), we simulate whole blood flow in a two-dimensional channel under a variety of flow conditions. A similar method has been used to study RBC deformation under shear-flow conditions by Sui, Chew & Low (2007). The immersed boundary (IB) method, created by Peskin (2002), is a specific way of coupling fluid dynamics to the mechanics of one or more objects located within the fluid. In our case, the elastic objects are RBC and platelet membranes. We treat the membrane of each cell as a thin, massless, elastic material and assume that the interior cytoplasm and surrounding plasma behave like incompressible Newtonian fluids. An

attractive feature of the IB method, in general, is that it does not require an explicit method to test for contact between the suspended IB objects. All interactions between the objects are mediated through the fluid and 'collisions' are not an issue. Because the velocity of each IB point (see (2.5)) matches that of the immediately adjacent fluid, two IB points which are initially at distinct locations cannot become co-localized at any later time. This implies that two disjoint IB objects, each represented by a closed curve, cannot interpenetrate. (This statement is for the continuous equations and for discretized versions provided the time step and the distance between the neighbouring IB points that make up each object's boundary are sufficiently small.)

The fluid dynamics are solved using the lattice Boltzmann equations (LBE) (see Ladd & Verberg 2001), which describe the evolution of fictitious microscopic particles on a discrete lattice whose dynamics depend on interactions between particle populations on neighbouring lattice points. At the macroscopic fluid scale, viscous flow dynamics emerge from these particle dynamics. The LBE in (2.1) are a second-order accurate approximation to the Navier–Stokes equations in the presence of a spatially varying, time-dependent force (see Guo, Zheng & Shi 2002; Crowl & Fogelson 2010). All lattice Boltzmann calculations are local ones, which makes parallelization straightforward and efficient. The variables of interest in the LBE are the density functions $f_i(\boldsymbol{x}, t)$ for particles at a lattice point $\boldsymbol{x}$ at time t and moving with the discrete velocity vectors $\boldsymbol{e}_i$. The governing equations for the particle density functions are

$$f_i(\boldsymbol{x} + \boldsymbol{e}_i \mathrm{d}t, t + \mathrm{d}t) - f_i(\boldsymbol{x}, t) = \frac{1}{\tau}\left(f_i(\boldsymbol{x}, t) - f_i^{eq}(\rho, \boldsymbol{v})\right) + w_i\, \mathrm{d}t \frac{(2\tau - 1)}{2\tau}\left[\frac{3(\boldsymbol{F}_f \cdot \boldsymbol{e}_i)}{c^2} + \frac{3\left(\boldsymbol{v}\boldsymbol{F}_f^T + \boldsymbol{F}_f\boldsymbol{v}^T\right) : \left(3\boldsymbol{e}_i\boldsymbol{e}_i^T - c^2\boldsymbol{I}\right)}{2c^4}\right]. \quad (2.1)$$

In the above equation $\mathrm{d}t$ is the time step, $c = h/\mathrm{d}t$ is the particle speed, τ is the non-dimensional relaxation time, $\boldsymbol{v}$ is the macroscopic velocity of the fluid and $\boldsymbol{F}_f$ is an external force felt by fluid. Equation (2.1) describes the two-step update procedure of the LBE. First, in the collision step, each particle distribution function relaxes towards a local equilibrium distribution, f_i^{eq}, at the rate $1/\tau$. Next, in the streaming step, the new distribution $f_i(\boldsymbol{x}, t)$ is advected from $\boldsymbol{x}$ at the corresponding velocity $\boldsymbol{e}_i$ to the lattice point located at $\boldsymbol{x} + \boldsymbol{e}_i\, \mathrm{d}t$. Nine discrete velocities are considered, and i ranges over the integers $0, \ldots, 8$. The nine equilibrium distributions are given by

$$f_i^{eq}(\rho, \boldsymbol{v}) = \rho w_i \left(1 + \frac{3\boldsymbol{e}_i \cdot \boldsymbol{v}}{c^2} + \frac{9(\boldsymbol{e}_i \cdot \boldsymbol{v})^2}{2c^4} - \frac{3\boldsymbol{v} \cdot \boldsymbol{v}}{2c^2}\right), \quad (2.2)$$

where the nine velocity vectors and corresponding equilibrium weights, w_i, are

$$\boldsymbol{e}_i = \begin{cases} (0, 0) \\ (c\cos(\pi(\mathrm{i} - 1)/4), c\sin(\pi(\mathrm{i} - 1)/4)) \\ c\sqrt{2}\cos(\pi(\mathrm{i} - 1)/4), c\sqrt{2}\sin(\pi(\mathrm{i} - 1)/4)) \end{cases} \qquad w_i = \begin{cases} 4/9 & \text{for } i = 0 \\ 1/9 & \text{for } i = 1, 3, 5, 7 \\ 1/36 & \text{for } i = 2, 4, 6, 8. \end{cases} \quad (2.3)$$

The equilibrium state at the lattice point $\boldsymbol{x}$ depends on the macroscopic quantities $\rho(\boldsymbol{x}, t)$ and $\boldsymbol{v}(\boldsymbol{x}, t)$ which approximate the macroscopic fluid density and velocity in the Navier–Stokes equations. In terms of the particle density functions, $f_i(\boldsymbol{x}, t)$, $\rho(\boldsymbol{x}, t)$ and $\boldsymbol{v}(\boldsymbol{x}, t)$ are defined by the formulas

$$\rho(\boldsymbol{x}, t) = \sum_i f_i(\boldsymbol{x}, t) \quad (2.4)$$

$$\rho(\boldsymbol{x},t)\boldsymbol{v}(\boldsymbol{x},t)-\frac{\mathrm{d}t\boldsymbol{F}_f}{2}=\sum_i f_i(\boldsymbol{x},t)\boldsymbol{e}_i, \tag{2.5}$$

respectively. Consistent with these definitions, pressure is defined by the adiabatic equation of state $p(\boldsymbol{x},t)=c_s^2\rho(\boldsymbol{x},t)$, where $c_s=c/\sqrt{3}$ can be interpreted as the speed of sound propagation in the fluid. Finally, the macroscopic fluid viscosity is given in terms of the relaxation time τ and other parameters by the formula $\mu=\rho c_s^2(\tau-\frac{1}{2})\,\mathrm{d}t$.

Positions of points on each elastic object are described by a Lagrangian variable $\boldsymbol{X}(q,t)$ which is not restricted to the Cartesian grid. Here, the variable q is taken to be the arclength along the object's boundary. The IB method enforces a no-slip condition on the elastic membranes. This requirement that each point moves at the same velocity as the immediately adjacent fluid can be expressed as

$$\frac{\partial\boldsymbol{X}}{\partial t}(q,t)=\boldsymbol{v}(\boldsymbol{X}(q,t),t)=\int\boldsymbol{v}(\boldsymbol{x},t)\delta(\boldsymbol{x}-\boldsymbol{X}(q,t))\,\mathrm{d}\boldsymbol{x}, \tag{2.6}$$

where $\delta(\boldsymbol{x})$ is the Dirac delta function.

Deformation of a cell generates elastic forces at each point $\boldsymbol{X}(q,t)$ of the membrane. Because we treat the membrane as massless, this force is transmitted to the adjacent fluid to give the quantity $\boldsymbol{F}_f$ in (2.1). The mathematical expression for the transmission of force from the elastic membrane to the fluid is given by the equation

$$\boldsymbol{F}_f(\boldsymbol{x},t)=\int\boldsymbol{F}_{IB}(q,t)\delta(\boldsymbol{x}-\boldsymbol{X}(q,t))\,\mathrm{d}q. \tag{2.7}$$

The force density applied to the fluid by the elastic membrane is concentrated spatially along the membrane. In order to determine what the IB force function $\boldsymbol{F}_{IB}(q,t)$ should be, we need to understand the behaviour of cellular membranes.

The RBC membrane is only a few molecules thick, and hence it is typically treated as one-dimensional with an inherent thickness. The elastic properties of a cellular membrane can be described by the Skalak tension law (see Skalak *et al.* 1973; Barthes-Biesel, Diaz & Dhenin 2002), developed specifically to describe the stress–strain relationship of RBC membranes.

$$T^{sk}=(\lambda^2-1)(G+K\lambda^2(\lambda^2+1)). \tag{2.8}$$

Here, G is the shear modulus and K is the area expansion modulus. In (2.8), $\lambda=\mathrm{d}q/\mathrm{d}q_{ref}$ represents the stretch ratio, where $\mathrm{d}q_{ref}$ is the length element prior to deformation and $\mathrm{d}q$ is the current length element. Since we represent membranes as one-dimensional objects, we must directly account for bending tension in order to recover realistic cellular rest shapes. The bending force acts in the normal direction and has magnitude

$$b=\frac{\mathrm{d}}{\mathrm{d}q}[E_B(\kappa(q)-\kappa_0)]. \tag{2.9}$$

Here, E_B is the bending modulus, κ is the instantaneous curvature and κ_0 is the curvature of minimum bending energy (see Pozrikidis 2001). The full equation for the IB force on an RBC membrane is therefore

$$\boldsymbol{F}_{IB}=\frac{\mathrm{d}\boldsymbol{T}}{\mathrm{d}q}=\frac{\mathrm{d}}{\mathrm{d}q}(T^{sk}t+bn), \tag{2.10}$$

where t and n are the unit tangent and normal to the membrane, respectively. Platelets circulate in an unactivated state in which they have an ellipsoidal shape and measure 1.5–3.0 μm in diameter. We construct approximately rigid circular platelets governed

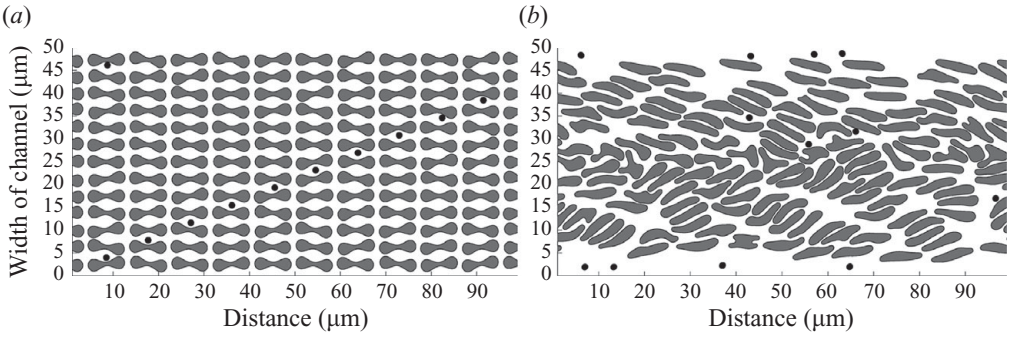

FIGURE 1. (*a*) The original set of simulations were initialized with a uniform lateral density of platelets and RBCs with biconcave rest shapes. (*b*) After 600 ms of flow a considerable amount of lateral transport is observed. These snapshots are taken from numerical experiments at 40 % haematocrit and a pressure gradient driven flow with a wall shear rate of $1100\,\mathrm{s}^{-1}$. Twelve platelets are included in each simulation since platelets account for only 0.3 % of blood by volume.

by (2.10) with a linear Hookean law for membrane tension $T^H = S(\lambda^2 - 1)$ replacing the Skalak law T^{sk} used for RBCs. More information about the lattice Boltzmann IB method can be found in Crowl & Fogelson (2010).

We use this method to study the behaviour of whole blood in a periodic, 50 μm wide channel. Flow in the channel is driven by a constant pressure gradient applied by adding a constant to the x-component of $\boldsymbol{F}_f$. No-slip boundary conditions are imposed at the channel walls using a second-order lattice Boltzmann bounce-back scheme (see He *et al.* 1997) at the lattice nodes directly adjacent to the wall boundaries. The fluid flow is initially set to the parabolic flow that would develop from the constant pressure gradient if there were no RBCs in the domain. Initial placement of RBCs and platelets will be described in the following section.

3. Results

3.1. *Effect of initial conditions*

In a recent paper (see Crowl & Fogelson 2010), we demonstrated lateral transport of platelets using a computational model of whole blood. The initial distributions of both RBCs and platelets were uniform in the domain, and after 600 ms of blood flow, platelets migrate into the cell-free layer (see figure 1). However, to conclude that lateral platelet motion is independent of initial conditions requires further analysis. In the original set of numerical simulations, two cellular redistributions occur simultaneously. First, RBCs migrate towards the centre of the vessel to a region of lower shear and create a RBC-free layer near the channel walls. Second, platelets get transported towards the vessel walls and create a sharply peaked concentration profile in this region. The migration of deformable droplets to regions of lower shear is a well-studied phenomenon, both analytically (see Wohl & Rubinow 1974; Chan & Leal 1979) and experimentally (see Goldsmith 1971; Goldsmith & Marlow 1972). In our two-dimensional 50 μm wide channel simulations with a wall shear rate of $1100\,\mathrm{s}^{-1}$, RBC inward migration occurs primarily during the first 300 ms (see figure 2). The near-wall excess of platelets begins to develop after the first 100 ms and continues to climb for an additional 900 ms.

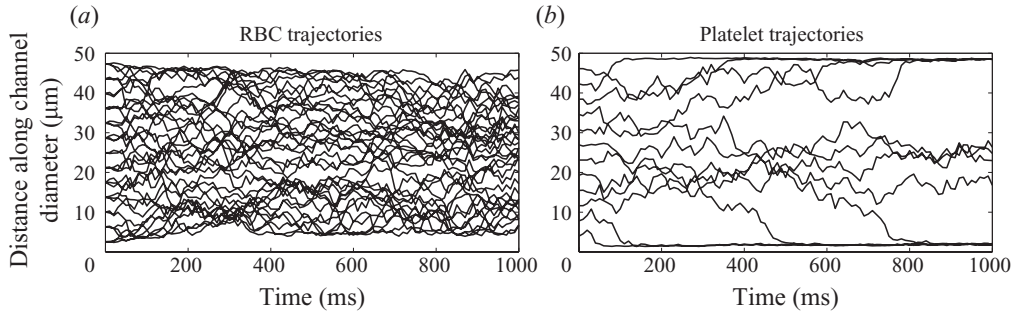

FIGURE 2. The lateral positions of RBC (*a*) and platelet (*b*) centres are plotted with respect to time over the course of a one second simulation. Initial conditions, haematocrit and wall shear rate are identical to those for figure 1.

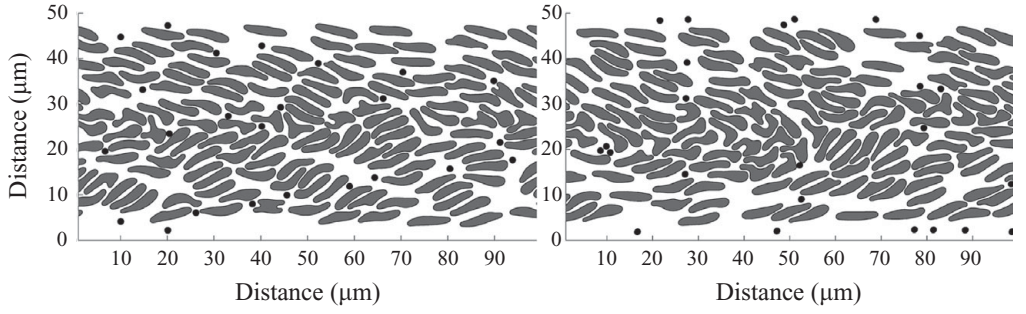

FIGURE 3. Simulations initialized with equilibrated RBCs and 24 laterally uniformly spaced platelets. These snapshots are taken under conditions of 40 % haematocrit at a wall shear rate of $1100\,\mathrm{s}^{-1}$ at 0 ms and 600 ms, respectively.

In order to determine whether platelet transport towards the vessel walls is a result of inward RBC motion simply displacing the plasma volume containing platelets, we conduct new numerical experiments in which the initial positions and shapes of the RBCs are taken to be the RBCs after 600 ms of flow starting from an initial set-up as in figure 1(*a*). Hence, the cell-free layer is already present at the start of the new simulations. Next, platelets are placed approximately uniformly across the channel within the empty space between RBCs (see figure 3). Whole blood simulations with this set-up are then run with flow driven by the same pressure gradient as the original set of simulations shown in figure 1. This second approach eliminates the coupling between RBC and platelet redistributions. We note that setting up such an experiment in a laboratory would pose a huge challenge.

The results presented in figure 4 indicate that the presence and extent of the platelet near-wall excess after 600 ms of blood flow are independent of the initial inward motion of RBCs. However, the initial conditions affect the time scale over which we see the development of a platelet near-wall excess, and evidence for this is shown in figures 5 and 6 for 40 % and 20 % RBC concentrations, respectively. In both cases, the equilibrated RBC initial conditions appear to promote faster platelet transport towards the vessel walls than our original choice of initial conditions. This is a non-intuitive result which may suggest that platelet transport occurs primarily as a result of natural interactions with RBCs in their equilibrated state. As the RBCs migrate towards the centre from a uniform distribution they may create a sieve effect,

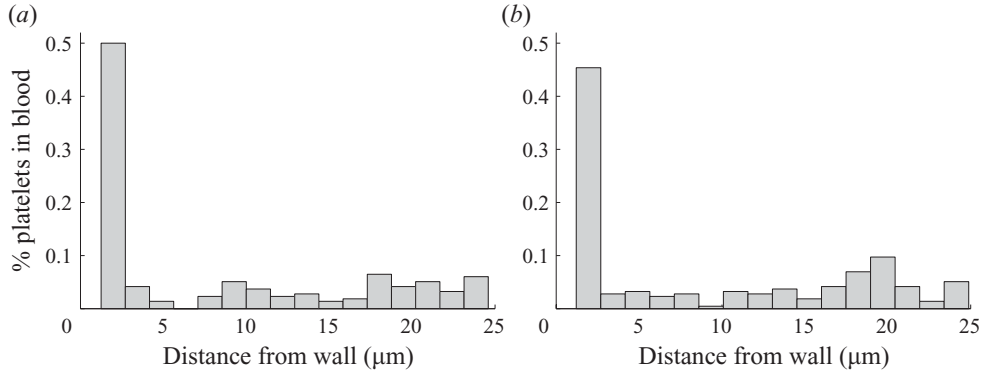

FIGURE 4. Initial conditions do not appear to effect the developed platelet-concentration profile. After platelets are allowed to redistribute under identical flow conditions of 40 % haematocrit and a wall shear rate of 1100 s^{-1} for 600 ms, both situations (figures 1 and 3) give rise to a peak-to-centre ratio above 8:1. (*a*) Initial conditions shown in figure 1. (*b*) Initial conditions shown in figure 3.

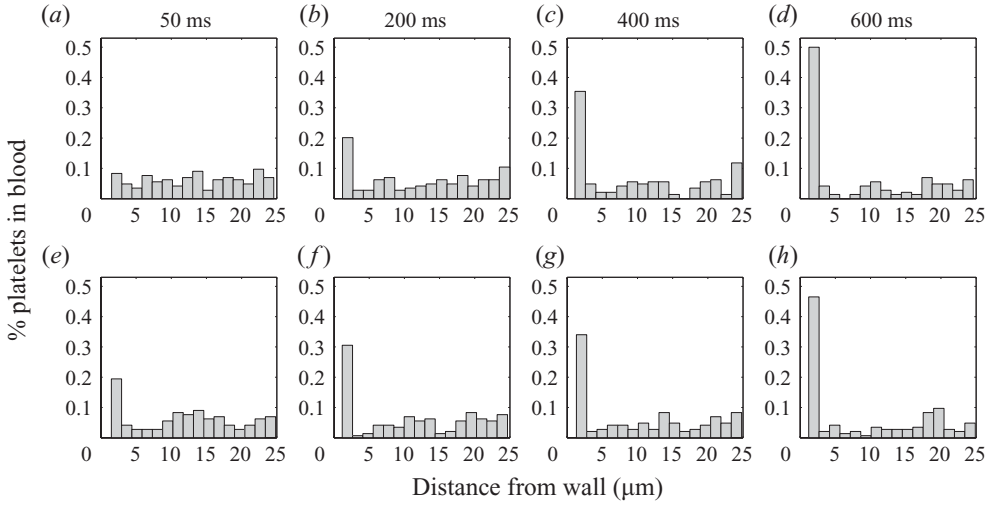

FIGURE 5. We plot histograms of platelet-concentration profiles at 50, 200, 400 and 600 ms for both the (*a–d*) original initial conditions in figure 1 and the (*e–h*) equilibrated RBC initial conditions in figure 3 at 40 % RBC suspensions with a wall shear rate of 1100 s^{-1}. Platelets exposed to an equilibrated RBC population for the total extent of simulation time develop a near-wall excess faster than platelets that are initially exposed to a uniform concentration of RBCs.

squeezing plasma out of the central region and dragging platelets along with them until the platelets escape through the available space between RBCs into the cell-free layer.

3.2. *Effect of haematocrit and flow rate*

The platelet-concentration peak for a normal human haematocrit of 40 % is tightly confined to a small near-wall region, and the peak-to-centre ratio is greater than 8 (see figure 4). In panels *d* and *h* of figure 6, we see that at 20 % haematocrit this peak is slightly wider and the peak-to-centre ratio is around half as high as in the

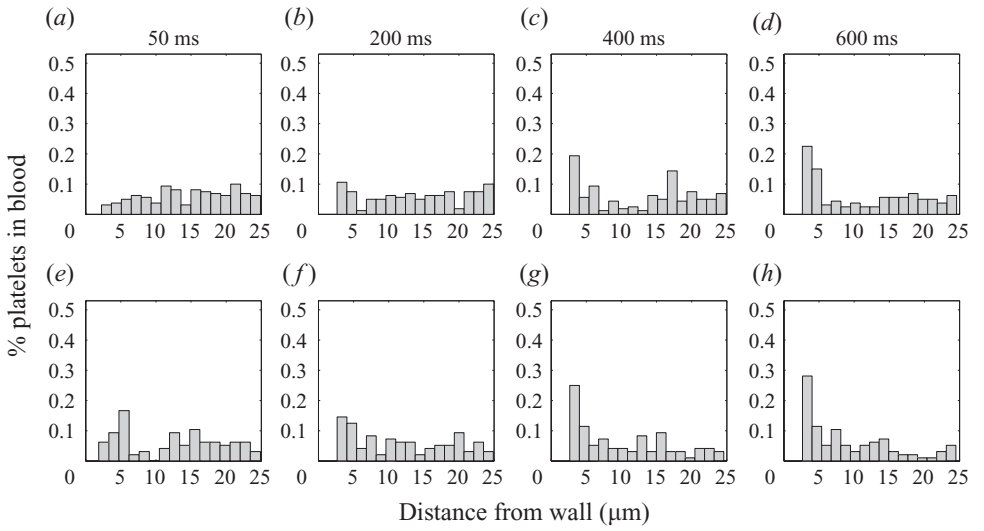

FIGURE 6. We plot histograms of platelet-concentration profiles at 50, 200, 400 and 600 ms for both the (*a–d*) original initial conditions in figure 1 and the (*e–h*) equilibrated RBC initial conditions in figure 3 at 20 % RBC suspensions with a wall shear rate of $1100\,\mathrm{s}^{-1}$. Platelets exposed to an equilibrated RBC population for the total extent of simulation time develop a near-wall excess faster than platelets that are initially exposed to a uniform concentration of RBCs.

40 % case. The differences between these platelet-concentration profiles are likely a direct result of the differences in the cell-free layers between haematocrits. The cell-free layer at 40 % haematocrit in our whole blood simulations has a thickness of 2–3 μm, whereas it is 5–6 μm wide for 20 % suspensions (see Crowl & Fogelson 2010).

It has been suggested by Koleski & Eckstein (1991) that wall shear rate may have a strong influence on the concentration profile of platelets. To investigate this relationship, we compare simulations driven by a pressure gradient that results in a wall shear rate of $400\,\mathrm{s}^{-1}$ to simulations driven by a pressure gradient three times larger, resulting in a wall shear rate of $1100\,\mathrm{s}^{-1}$. For our whole blood model, we have direct control over the pressure gradient driving the flow, and the same pressure gradient results in approximately the same wall shear rate for both haematocrit cases since there are no RBCs at the wall. The shear rate across the channel diameter, provided in figure 7, is small and nearly linear in the central region of the vessel where the RBCs reside and much larger in magnitude outside of this region. At the wall there is no significant difference in the shear rate between the two haematocrits. On the other hand, the average velocity differs between haematocrits. For the same pressure gradient resulting in a wall shear rate of $1100\,\mathrm{s}^{-1}$, the 20 % blood suspension has an average velocity of $0.87\,\mathrm{cm\,s}^{-1}$, whereas the 40 % suspension has an average velocity of only $0.64\,\mathrm{cm\,s}^{-1}$. In whole blood, the fluid velocity profile matches a parabolic flow near the vessel walls, but the high density of RBCs at the centre causes the velocity to have a flattened, plug-like profile near the centre of the channel. This effectively slows down the fluid velocity at the centre of the channel and results in a smaller average velocity.

Figure 8 shows a time progression of platelet distribution from a uniform profile over the course of 1.8 s under $400\,\mathrm{s}^{-1}$ wall shear rate flow conditions with 20 % and 40 % blood suspensions. After the low wall shear rate simulations have run

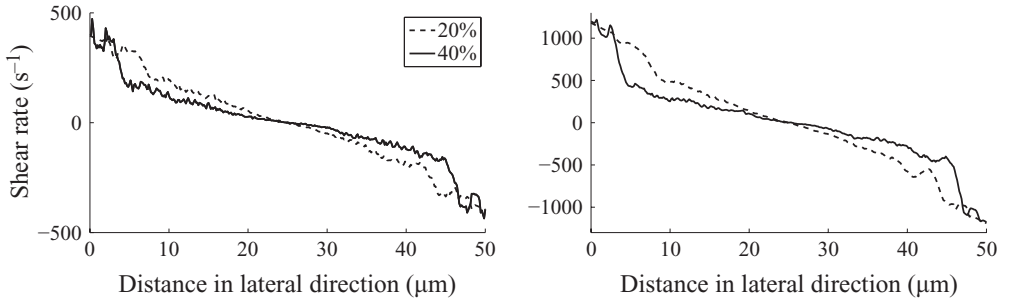

FIGURE 7. The shear rate along the lateral direction for 20 % and 40 % haematocrits for both the low and high flow conditions is approximately linear at the centre of the channel, with a jump in magnitude near the domain walls. The shear rate is averaged along the axial direction and in time from 400–600 ms of flow.

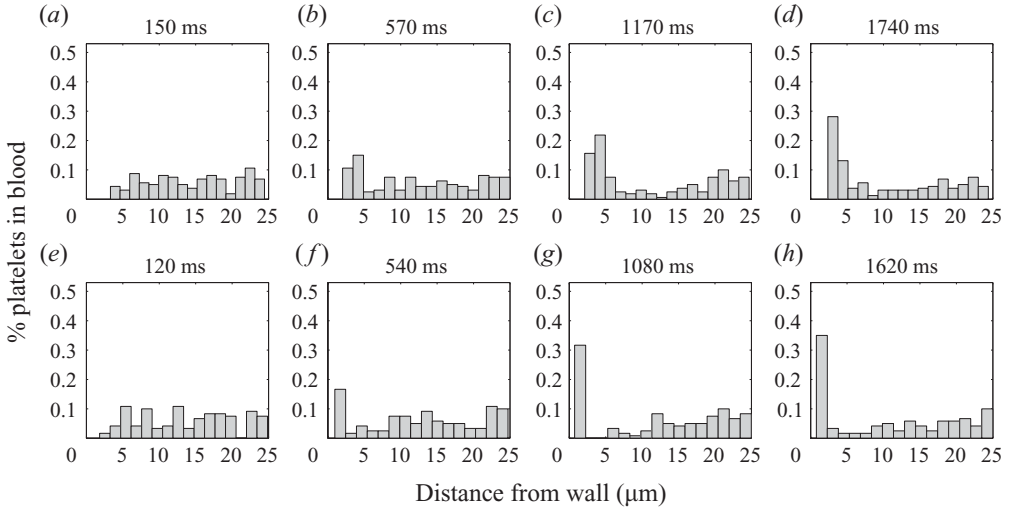

FIGURE 8. Platelet concentration is plotted as a function of lateral position over the course of 1740 ms for a low wall shear rate of 400 s^{-1} and 20 % haematocrit (*a–d*) and 1620 ms for the same wall shear rate and 40 % haematocrit (*e–h*). Comparison with the corresponding panels in figures 5 and 6 reveals that the rate of platelet transport to the RBC-free layer is approximately proportional to the flow rate. The ratios between average velocities between low and high wall shear rate simulations are 2.88:1 for the 20 % case and 2.68:1 for the 40 % case.

for approximately 600 ms, a much smaller near-wall excess is observed compared to the high wall shear rate simulations (figures 5–6) after the same amount of time. For the low wall shear rate at 20 %, we see a peak-to-centre ratio of 3:1 versus 5:1 for the high wall shear rate and 4:1 versus 9:1 for 40 %. However, on average, platelets in the high wall shear case have travelled further along the channel than platelets in the low wall shear rate situation. Using average flow rates, we predict that on average platelets move 2.88 times further for 20 % blood suspensions at the higher wall shear rate and 2.64 further for 40 % blood suspensions. To correct for this difference, we compare platelet profiles at the same 'distance' along the vessel. For example, we compare the high wall shear rate simulations after 200 ms and 600 ms to the low wall shear rate after 570 ms and 1740 ms for the 20 % haematocrit blood suspension simulations. This comparison reveals that the peak-to-centre ratios are fairly similar after the

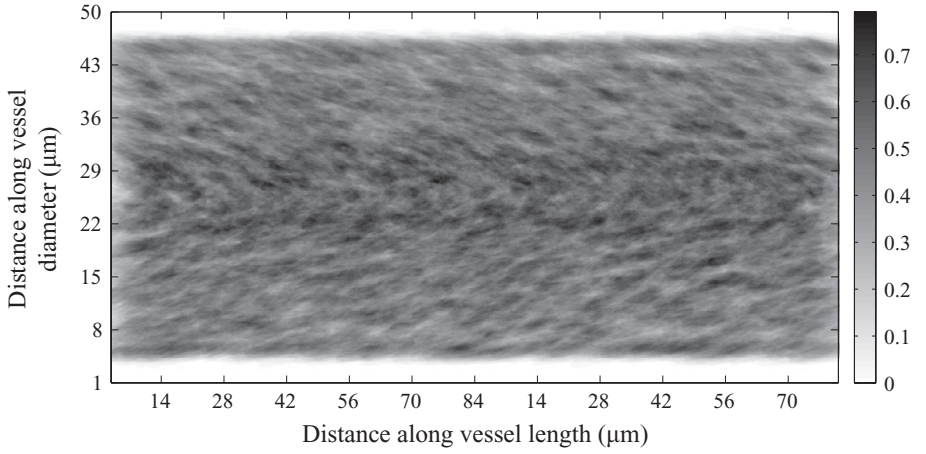

FIGURE 9. Under arterial flow conditions, RBCs drift towards the centre of a vessel. This plot shows the effective density of simulated red cells averaged over 600 ms in a 50 μm wide, 2D vessel at 40 % haematocrit and a wall shear rate of $1100\,s^{-1}$. Instead of the entire domain being at a red cell density of 40 %, there are no red cells in the regions within 3 μm of the walls and the density is about 50 % near the vessel centre.

same 'distance' travelled for the 20 % haematocrit case. For 40 % RBC concentration, the high wall shear rate channel flow produces a slightly larger near-wall excess even when platelets in the low wall shear rate simulations are allowed to migrate three times longer (1800 ms instead of 1620 ms, histogram not shown). Thus, it appears that platelet transport may be proportional to the wall shear rate for low concentrations of RBCs, but the nature of the shear rate dependence becomes less clear as blood becomes thicker and the flow dynamics become more complex.

3.3. *Accounting for volume exclusion*

Volume exclusion due to RBCs at the centre of the vessel certainly contributes to the non-uniform concentration profile of platelets in flowing whole blood. To what extent it contributes is unclear and is the reason for our investigation in this section. Let us temporarily assume that platelets are passive objects that occupy the empty space around RBCs. If platelets were infinitesimally small and their motion was governed by a pure diffusion process, they would fill this empty space uniformly at equilibrium. This in itself would create a high near-wall concentration profile due to the fact that under arterial flow conditions, there is a RBC-free layer near the wall. Highly deformable droplets, such as RBCs, are known to migrate towards the regions of lowest shear (see Goldsmith 1971). Therefore, when exposed to flow in a channel driven by a pressure gradient, RBCs migrate radially inward and produce a RBC-free layer near the channel walls. Figure 9 illustrates the RBC-free layer in our simulations at 40 % haematocrit and a wall shear rate of $1100\,s^{-1}$.

Moreover, the excluded volume due to RBCs should be larger for platelets of finite size, since platelet cells' centres cannot be located directly adjacent to RBC membranes due to their non-zero radii. We can estimate the extent of excluded volume increase due to platelet size by including a boundary layer around each RBC with thickness equal to the platelet radius (see figure 10). We define the percentage of space available to platelets as the average per cent of space that is at least a platelet radius away from any RBC in the domain. The per cent of available space for platelets at 20 % and 40 % haematocrit as a function of lateral position is presented in figure 11.

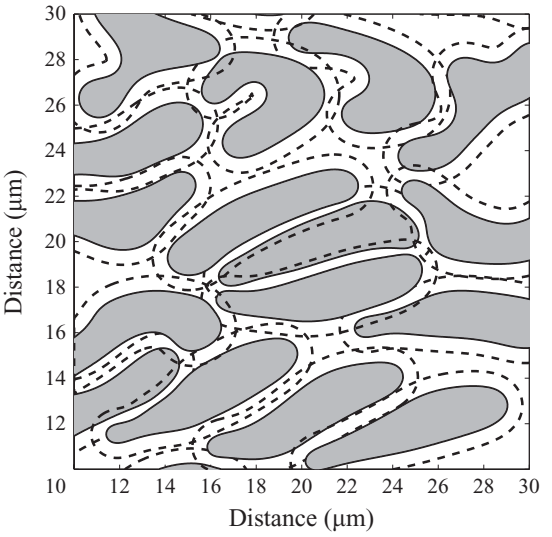

FIGURE 10. To calculate the additional volume exclusion due to the platelet size around red cells, a layer of thickness equal to a platelet radius is added around the boundary of each red cell.

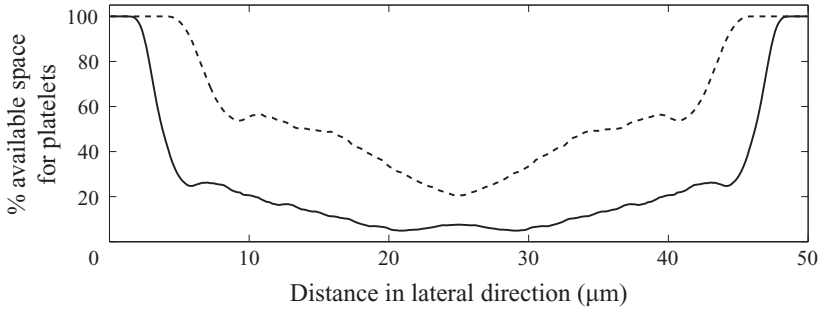

FIGURE 11. We average over time and axial position to calculate the approximate percentage of space available to platelets in 20 % (dashed line) and 40 % (solid line) suspensions under the flow conditions with a wall shear rate of $1100\,s^{-1}$ as a function of the distance from the centre of the channel. We define the percentage of available space to be the average per cent of space available to platelets with finite radii (as in figure 10).

Figure 12 illustrates the degree to which excluded volume accounts for the platelet near-wall excess in our numerical experiments. We present platelet concentration as a function of lateral position next to profiles of platelet concentration in plasma and platelet concentration in the available space around RBCs in which we take into account the platelet radius with an additional RBC boundary layer (see figure 10). Since the available space at the centre of the domain is only 10 % of the total space (and 100 % in the RBC-free layer at the wall in figure 11), the peak-to-centre ratio of 10:1 in figure 4 drops to the 1:1 ratio. It is apparent that this excluded volume calculation creates much less pronounced concentration profiles; however, the available space argument does not fully account for the non-uniform platelet distributions that we find in our simulation data. Excluded volume would predict a constant platelet density within the available space after a sufficiently long time, and instead we see a dip in the region between the cell-free layer and the channel centre. Koleski & Eckstein (1991) also came to the conclusion that volume exclusion is not

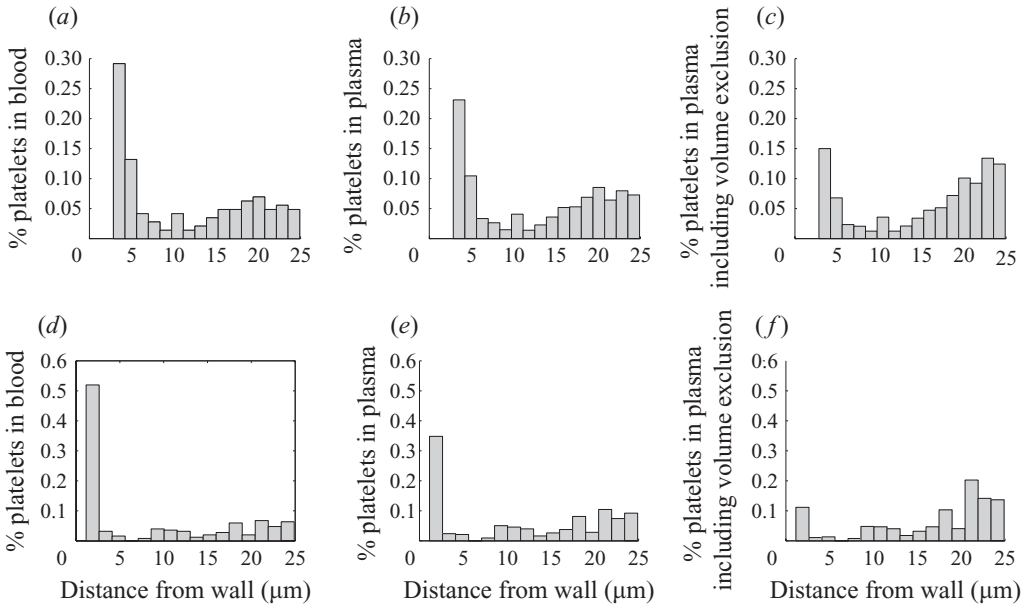

FIGURE 12. Accounting for volume exclusion for platelet-concentration data at 20 % (*a–c*) and 40 % (*d–f*) haematocrit and a wall shear rate of $1100\,\mathrm{s}^{-1}$ after 600 ms of flow. (*a*, *d*) Concentration of platelets per unit total volume as a function of lateral position. (*b*, *e*) Concentration of platelets per unit plasma volume (accounting for the presence of RBCs, but not non-zero platelet radii) as a function of lateral position. (*c*, *f*) Concentration of platelets per unit available space at least a platelet radius away from any RBC surface as a function of lateral position. The available space is estimated from averaging RBC density data between 400 and 600 ms of flow.

sufficient to explain platelet behaviour after comparing smaller near-wall excesses of platelets at 60 % haematocrit suspensions to higher peak-to-centre ratios in 40 % suspensions. Another shortcoming to the volume exclusion argument is that a back-of-the-envelope calculation for the redistribution time of platelets due to Brownian motion ($D = 10^{-9}\,\mathrm{cm}^2\,\mathrm{s}^{-1}$, Goldsmith 1971) is on the order of an hour. On the other hand, if RBCs induce a sufficiently large diffusion-like motion of platelets, the time scale could be much shorter as in our simulations.

To further examine the effect of volume exclusion on platelet behaviour, we investigate how platelet size plays a role by simulating whole blood with smaller platelets of diameter 0.75 μm. Our numerical experiments thus far have assumed a platelet diameter of 1.5 μm. Both sets of simulations are run with identical equilibrated RBC suspensions and equal numbers of platelets placed within the empty space at identical initial centres of mass. Theoretically, in the limit that platelet diameter approaches zero, the particles should move to fill the available space in the channel uniformly in time. Figure 13(*a*) shows that the smaller platelets develop a smaller near-wall excess. However, when the effects of volume exclusion due to platelet size are taken into account (see figure 13*c*), we see that the distribution of platelets in the available space is approximately independent of the platelet size. Both available space concentration profiles still show a dip between the near-wall region and the centre, which is not explained by the volume exclusion argument. A possible explanation for the dip is discussed in § 3.7. These profiles also show a high platelet concentration at the centre of the channel. It is possible that the high concentration at the channel

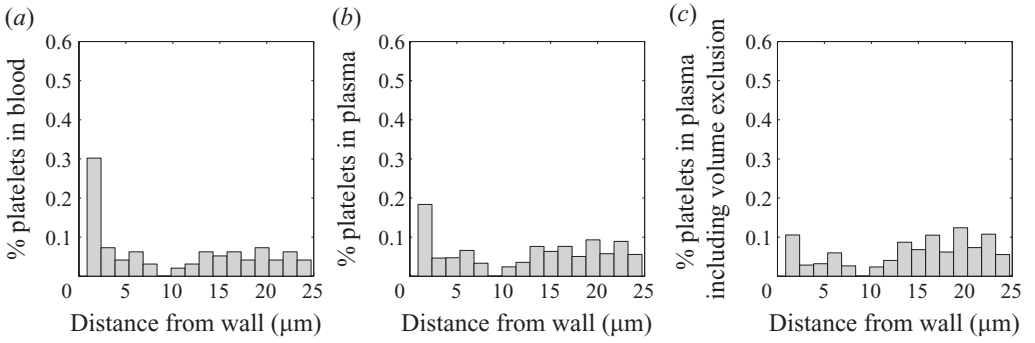

FIGURE 13. Concentration of small platelets (with diameter 0.75 μm) is plotted against the distance from the wall. (*a*) Concentration of platelets in whole blood, (*b*) in plasma and (*c*) in available space. Blood conditions are 40 % haematocrit and a wall shear rate of $1100\,\mathrm{s}^{-1}$. Histograms are plotted after 600 ms of simulated flow starting from equilibrated RBC initial conditions.

centre is a result of the non-uniform initial concentration of platelets in the available volume.

3.4. *Quantifying platelet diffusion*

Suppose that lateral platelet motion can be described by the Langevin equation for a stochastic drift–diffusion process,

$$\mathrm{d}y = A(y)\,\mathrm{d}t + B(y)\,\mathrm{d}W, \tag{3.1}$$

where $A(y)$ and $B(y) = \sqrt{D(y)}$ are the functions of lateral position in the domain. The Fokker–Planck equation

$$\frac{\partial P(y,t)}{\partial t} = \frac{\partial}{\partial y}\left(A(y)P(y,t) + \frac{1}{2}\frac{\partial D(y)P(y,t)}{\partial y}\right) \tag{3.2}$$

describes the corresponding probability density function (see Gardiner 2004). For such a process, we can recover the lateral drift A and diffusion D in the Langevin equation by computing the first two moments of (3.1) with respect to $\mathrm{d}W$,

$$\langle dy\rangle = A(y)\,\mathrm{d}t \tag{3.3}$$

$$\langle dy^2\rangle = D(y)\,\mathrm{d}t + o(\mathrm{d}t). \tag{3.4}$$

If we assume that platelet motions in our whole blood simulations are well described by such a drift–diffusion model, we can estimate $A(y)$ and $D(y)$ for platelets as follows. We partition the simulated time into intervals of $\Delta t = 10$ ms. We note the lateral position y of each platelet's centre of mass at the start of each time interval and the change in this position, $\Delta y(y)$, over the time interval. We then average $\Delta y(y)$ and $(\Delta y(y))^2$ along the domain (using a Savitzky & Golay 1964 filter, S-G filter hereafter) and by using the averages in (3.3) and (3.4), we estimate $A(y)$ and $D(y)$.

Turitto *et al.* (1972) experimentally estimated the enhanced diffusion of platelets due to RBCs in whole blood to be of the order of $10^{-7}\,\mathrm{cm}^2\,\mathrm{s}^{-1}$ for wall shear rates between 40 and $440\,\mathrm{s}^{-1}$. However, tracking actual platelet trajectories in the presence of RBCs is not yet experimentally feasible and this is where our numerical experiments can provide important insight. Using our numerical platelet trajectory data to compute the effective diffusive motion, we find that the enhanced diffusion of platelets due to interactions with RBCs at the centre of the channel may be as

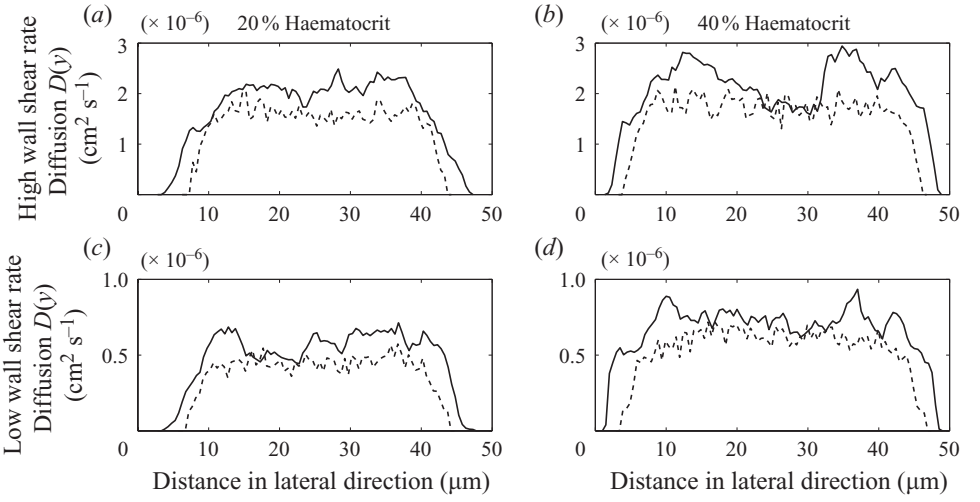

FIGURE 14. Diffusion is measured as a function of lateral position for both platelets (solid line) and RBCs (dashed line). These coefficients are estimated from platelet simulation data at 20 % and 40 % haematocrits and wall shear rates of $400\,s^{-1}$ and $1100\,s^{-1}$. The coefficients are calculated by averaging platelets' and RBCs' motions over the domain in the axial direction and over 250–600 ms of simulation time.

large as $2 \times 10^{-6}\,cm^2\,s^{-1}$ for high flow conditions (see figure 14*a*, *b*). It is also clear from figure 14 that platelet diffusion is non-uniform in the lateral direction; it drops off sharply in the cell-free layer. The peak platelet concentration is located at the boundary of the RBC-free layer which also corresponds to the steep gradient in diffusion. Such a variable diffusion coefficient in the Fokker–Planck sense drives the probability density to a non-uniform equilibrium in which the density is highest in the regions of low diffusion.

Our numerical results suggest that RBC-induced platelet diffusion increases with the shear rate since an increase in the wall shear rate from 400 to $1100\,s^{-1}$ translates to about a threefold increase in diffusion (compare figure 14*a*, *b* to figure 14*c*, *d*). Diffusion also increases with haematocrit both in the sense that the region of larger magnitude extends further towards the channel walls and in the sense that the magnitude of diffusion increases within the central region of the domain. In addition to platelet diffusion, we plot the diffusion of RBCs for a variety of flow conditions in figure 14 and find that it is of the same order as that of the platelet diffusion, though slightly smaller. This decrease in magnitude is most likely due to the larger size of RBCs, since their cellular velocity is an average over the fluid velocity in a broader region than platelets.

In order to gain information about cellular drift velocities from our whole blood model, we also calculate the drift of RBCs and platelets as a function of lateral position in figure 15. We see an RBC drift towards the centre of the channel for all flow conditions. In the 40 % haematocrit case at a high wall shear rate (see figure 15), we see what could be a platelet drift away from the wall. However, in general, our estimates for the platelet drift are very noisy and inconclusive. An accurate function for the platelet drift is difficult to recover from our simulation data due to the high level of diffusion at the centre of the channel and the small amount of platelet data compared to RBC data. Qian, Sheetz & Elson (1991) have estimated the error in drift

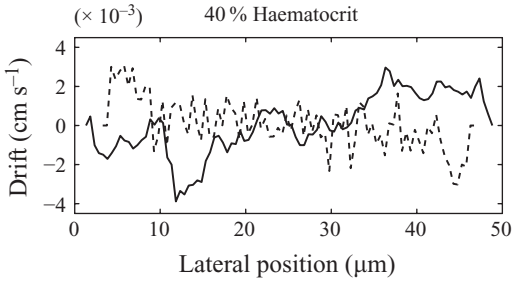

FIGURE 15. Drift ($\mathrm{cm\,s^{-1}}$) is measured as a function of lateral position across the vessel diameter for both platelets (solid line) and RBCs (dashed line). These coefficients are estimated from platelet simulation data at 40 % haematocrit and wall shear rate $1100\,\mathrm{s^{-1}}$. Estimated drift functions for 20 % haematocrit and shear rate $1100\,\mathrm{s^{-1}}$ (not shown) are similar in magnitude. Estimated drift functions for 20 % and 40 % haematocrit and shear rate $400\,\mathrm{s^{-1}}$ (not shown) are similarly noisy and have magnitude about half of that shown.

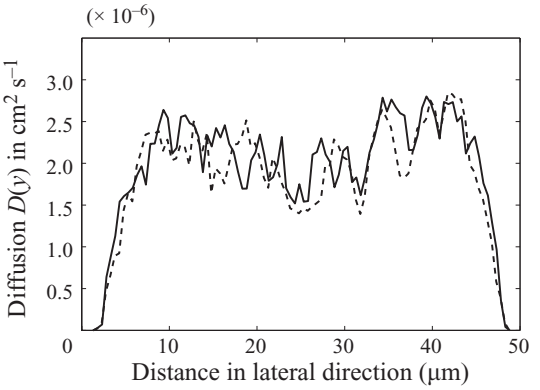

FIGURE 16. Diffusion for two different sized platelets (1.5 or 0.75 μm in diameter) at 40 % haematocrit and a wall shear rate of $1100\,\mathrm{s^{-1}}$. There is no significant difference between enhanced diffusion of small platelets compared to normal sized platelets.

velocity given a diffusion coefficient to be

$$Error(A) \approx \sqrt{\frac{4D}{N\Delta t}}. \tag{3.5}$$

For our simulations with a diffusion coefficient as large as $D = 2 \times 10^{-6}\,\mathrm{cm^2\,s^{-1}}$, $N \approx 4000$ data points and time step $\Delta t = 0.01$ s, this estimate gives us a drift velocity error of roughly $4 \times 10^{-4}\,\mathrm{cm\,s^{-1}}$, which is comparable to the estimated drift coefficients shown in figure 15. This is also most likely an underestimate of the error since RBC-induced platelet diffusion varies in time in addition to spatial location.

The diffusion for two different sized platelets (1.5 or 0.75 μm in diameter) is shown in figure 16. The platelet diffusion profile for small platelets is strikingly similar to normal sized platelets (both sets of simulations were initialized with identical equilibrated RBC suspensions and initial platelet positions, and this correlation may contribute to the extreme similarity in drift and diffusion calculations). This suggests that unlike classic diffusion, this enhanced 'diffusion' of platelets is a function of RBC dynamics, not of platelet characteristics.

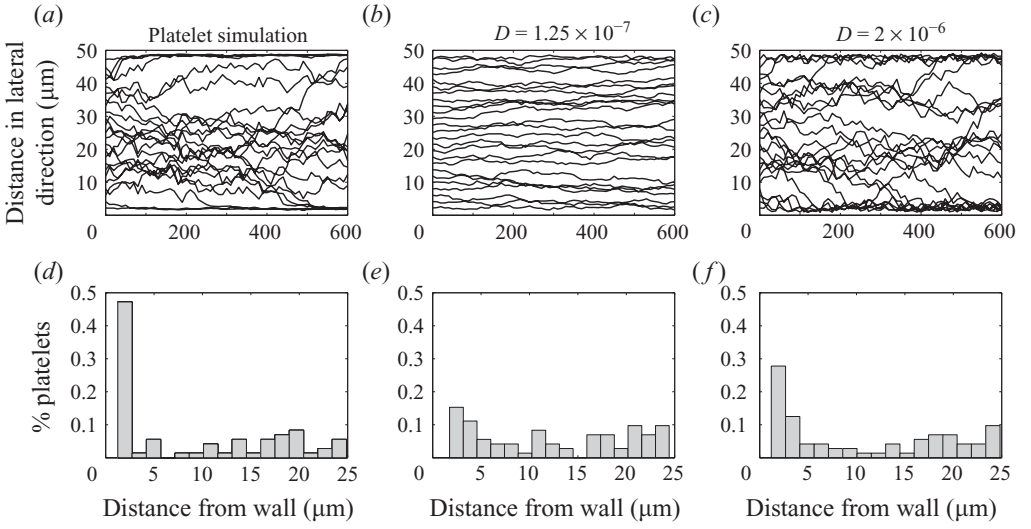

FIGURE 17. Platelet trajectories from our numerical experiment at 40 % haematocrit at a wall shear rate of $1100\,\mathrm{s}^{-1}$ and RBCs initialized at equilibrium as in figure 3. Stochastic differential equation simulations for a platelet drift–diffusion process (Eckstein & Belgacem 1991; Yeh *et al.* 1994). (*a–c*) Constant diffusion coefficient $D = 1.25 \times 10^{-7}\,\mathrm{cm}^2\,\mathrm{s}^{-1}$ and drift function $A(y) = Dc'_{eq}/c_{eq}$. The magnitude of this diffusion coefficient is an estimate of enhanced diffusion of platelets (see Eckstein & Belgacem 1991). (*d–f*) Higher diffusion coefficient of $D = 1.25 \times 10^{-6}\,\mathrm{cm}^2\,\mathrm{s}^{-1}$. Histograms are taken after 600 ms of simulated lateral platelet motion.

3.5. *Drift–diffusion model for platelet motion*

Because of the uncertainty in our estimation of the drift function in the previous section, we examine whether stochastic differential equation (SDE) models with our estimated diffusion coefficients can reproduce the platelet behaviour we see in our whole blood simulations, or if an additional drift is required. A similar approach was implemented by Eckstein & Belgacem (1991), who created a phenomenological drift–diffusion model to capture non-uniform platelet concentrations found experimentally by Tilles & Eckstein (1987) and Eckstein, Tilles & III (1988). Eckstein & Belgacem (1991) used the equation of lateral motion

$$\frac{\partial c(y,t)}{\partial t} = \frac{\partial}{\partial y}\left(A(y)c(y,t) + D\frac{\partial c(y,t)}{\partial y}\right) \tag{3.6}$$

for the concentration of platelets. They assumed a constant diffusion coefficient D and created an artificial drift term $A(y)$ such that the resulting equilibrium concentration of platelets, c_{eq}, matched the platelet equilibrium distribution from experimental data:

$$A(y) = D\left(\frac{\dfrac{\partial c_{eq}}{\partial y}}{c_{eq}}\right). \tag{3.7}$$

Note the Fickian form of the diffusion term in (3.6). It differs from the form in the Fokker–Planck (3.2) that is associated with the SDE 3.1 unless the diffusion coefficient is constant.

With our numerical model, we are able to track the paths of individual platelets in flowing blood suspensions and gain a more accurate representation of platelet motion (see figure 17). We can compare our platelet trajectories to SDE simulations

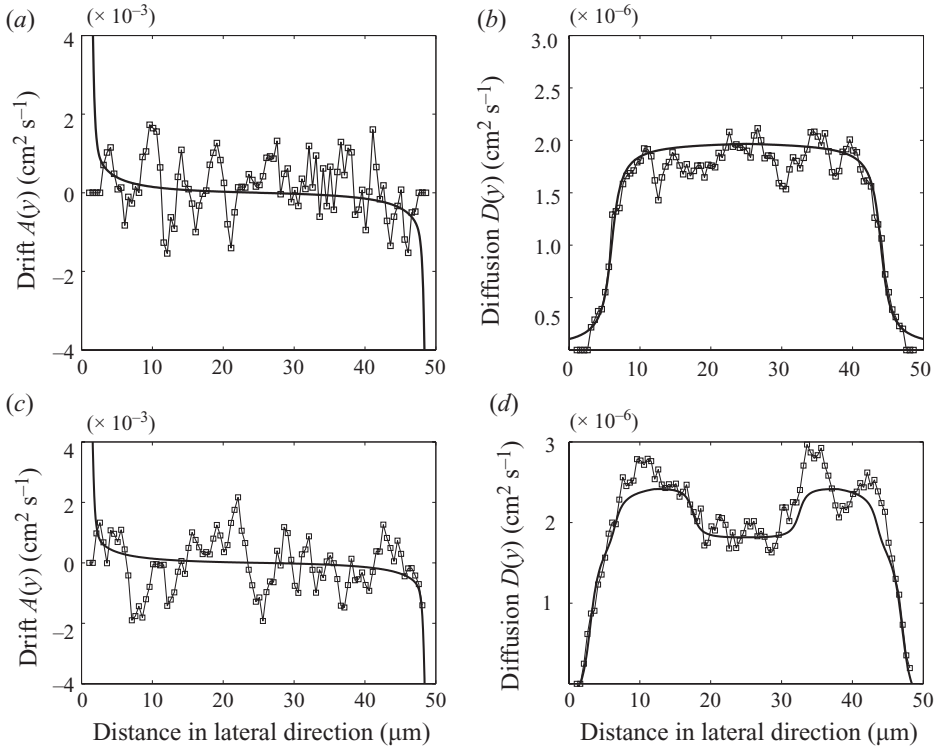

FIGURE 18. The smooth solid lines represent the diffusion and drift terms defined in (A 1) and (A 4) (a, b; for 20 % haematocrit) and (A 2) and (A 4) (c, d; for 40 % haematocrit) we use to approximate platelet behaviour at 20 % haematocrit and a wall shear rate of 1100 s^{-1}. We then use these functions to run SDE simulations for the same number of platelets we studied in our whole blood simulations and recover the drift and diffusion functions using the same approach used to estimated them from our whole blood model.

of the Eckstein & Belgacem (1991) drift–diffusion model. Using a constant diffusion coefficient of 1.25×10^{-7} cm^2 s^{-1} (see Eckstein & Belgacem 1991), the drift–diffusion model drastically underestimates platelet fluctuations at the centre of the channel (compare whole blood data in figure 17*a* to SDE data in figure 17*b*). In addition, SDE simulations with this value of D predict a much smaller near-wall excess after 600 ms than seen in our whole blood simulations.

In order for the SDE simulations to reproduce the near-wall excess, we see in whole blood simulations after 600 ms for a 40 % haematocrit suspension, the drift and hence the diffusion coefficient must be more than an order of magnitude larger than that assumed by Eckstein & Belgacem (1991). With a larger constant diffusion coefficient, the SDE trajectories overestimate the platelet fluctuations near the channel walls (see figure 17*c*), and so it appears that choosing a variable diffusion coefficient may be a more realistic approach to platelet drift–diffusion models.

3.6. *Stochastic differential equation for platelet motion*

In this section, we discuss simulations based on the SDE (3.1) where we think of y as the lateral location of a platelet centre. For the simulations, we use smooth diffusion functions (see figure 18 and Appendix A) fit to the estimated platelet diffusivity extracted from our whole blood flow simulations as described in § 3.4. We

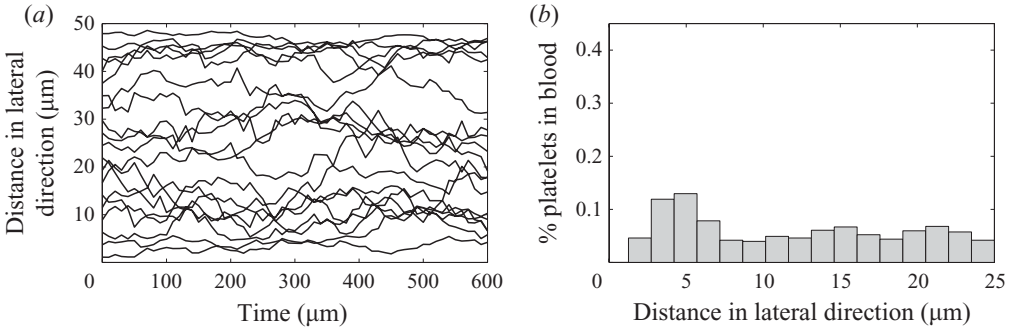

FIGURE 19. Plot of sample SDE trajectories and histogram of SDE platelet-concentration profile after 600 ms simulations started with uniform distibution of platelets at 20 % haematocrit using drift and diffusion (A 1) and (A 4) shown in the top panels of figure 18.

use separate smooth functions for 20 % and 40 % suspensions at a wall shear rate of $1100\,\mathrm{s}^{-1}$.

Our estimated drift function from the whole blood flow simulations is inconclusive, so we assume for now that there is no net drift due to RBCs in the channel. However, since platelets in the SDE simulations have no size, we explicitly include a wall-repulsion drift function to prevent them from contacting the wall. This drift extends slightly beyond the radius of a platelet because in the absence of RBCs, platelets drift away from a wall (see Goldman, Cox & Brenner 1967; McLaughlin 1993; Hu & Joseph 1999). We approximate the drift due to wall repulsion from platelet motion simulations in the absence of RBCs using our lattice Boltzmann-immersed boundary model (platelet trajectories shown in figure 10*a* in Crowl & Fogelson 2010). These smooth functions for both diffusion and drift are shown in figure 18 and the exact choices for $D(y)$ and $A(y)$ are given in Appendix A.

We discretize our SDE using an Euler procedure and use reflection boundary conditions at the walls of the domain. We run a series of SDE simulations with these prescribed drift and diffusion functions for both the 20 % and 40 % cases. These SDE simulations involve particles initially placed uniformly in the domain and run for 600 ms each. We then recover approximations to our drift and diffusion from this SDE data using the same method, number of data points and filtering that we used for platelet data gathered from the numerical whole blood model. We see that the diffusion function is recovered fairly well, but once again the drift function is very noisy and inconclusive.

We present stochastic simulations of these drift–diffusion models in figures 19 and 20, for 20 % and 40 % haematocrit respectively. The histograms obtained from these SDE simulations suggest that this combination of variable diffusion and wall repulsion is not enough to obtain the peak-to-centre ratios that we see after 600 ms of flow in our whole blood model (see figure 12).

3.7. *Evidence for an additional drift*

Together, our whole blood simulation data and the SDE simulations argue for an additional drift term that forces platelets out of the region adjacent to the RBC-free layer. A possible physical rationale for this additional outward drift concerns the biased orientation of RBCs in the flow. Figure 21 shows the mean and variance of RBC orientation in our whole blood simulations at 40 % haematocrit and a wall shear rate of $1100\,\mathrm{s}^{-1}$ as a function of lateral position in the domain. The orientation

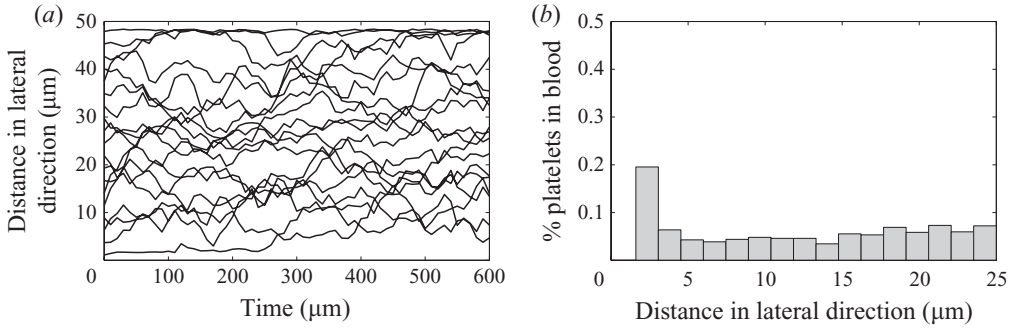

FIGURE 20. Plot of sample SDE trajectories and histogram of SDE platelet-concentration profile after 600 ms started with uniform distibution of platelets at 40 % haematocrit using drift and diffusion equations (A 2) and (A 4) shown in the bottom panels of figure 18.

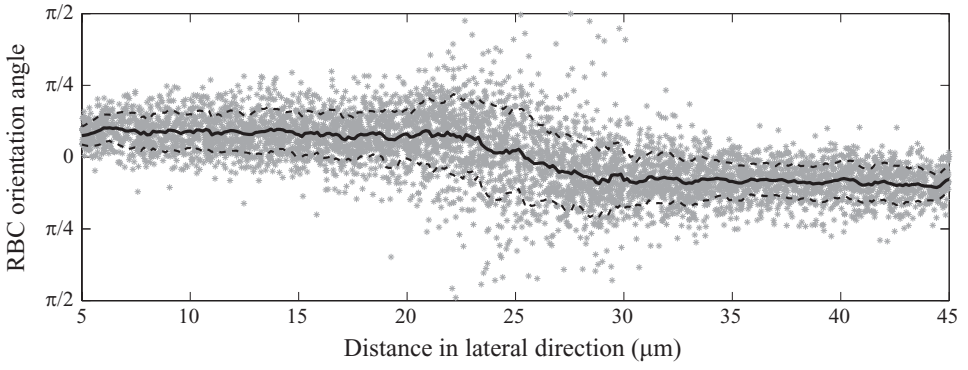

FIGURE 21. Mean and variance of RBC orientation in flow at 40 % haematocrit and a wall shear rate of $1100\,\mathrm{s}^{-1}$ are calculated from whole blood simulations for equilibrated RBCs.

of each RBC is calculated as the angle between the axial direction and the principal axis of the second moment,

$$M_2 = \int_V \begin{bmatrix} x \\ y \end{bmatrix} [x\ ,\ y] \rho(x, y)\, \mathrm{d}V, \tag{3.8}$$

where x and y denote the position relative to the cell's centre of mass and $\rho(x, y)$ is unity in the interior of an RBC and zero outside.

It is a well-known phenomenon that under shear-flow conditions, RBCs take on an elliptical shape with a set orientation angle and exhibit a behaviour known as tank-treading (see Fischer, Stohr-Lissen & Schmid-Schonbein 1978; Eggleton & Popel 1998; Sui *et al.* 2007). The membrane rotates around the internal fluid, while the shape of the RBC remains constant. In shear flow, when a platelet comes into contact with a tank-treading RBC with an orientation angle as in figure 22, the platelet is forced up or down (depending on direction of shear and relative lateral position) as the RBC approaches. In most regions of the flow in our whole blood simulations, platelets are pushed both up and down because there are approximately equal numbers of RBCs above and below them. This is not true in the region bounding the cell-free layer, where the concentration of RBCs is not uniform in the lateral direction. In this slice of the domain, RBCs may act as an effective barrier to platelets in the cell-free layer due to their preferred orientation angle. For example, if a platelet is just below the cell-free layer, it will feel a directed force away from the RBCs.

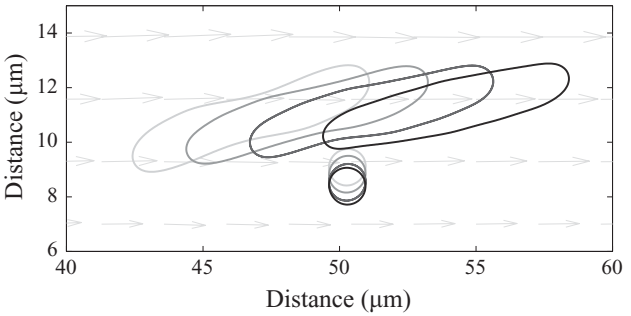

FIGURE 22. An example of directed motion: the RBC's orientation angle forces the platelet down as they encounter each other under shear-flow conditions.

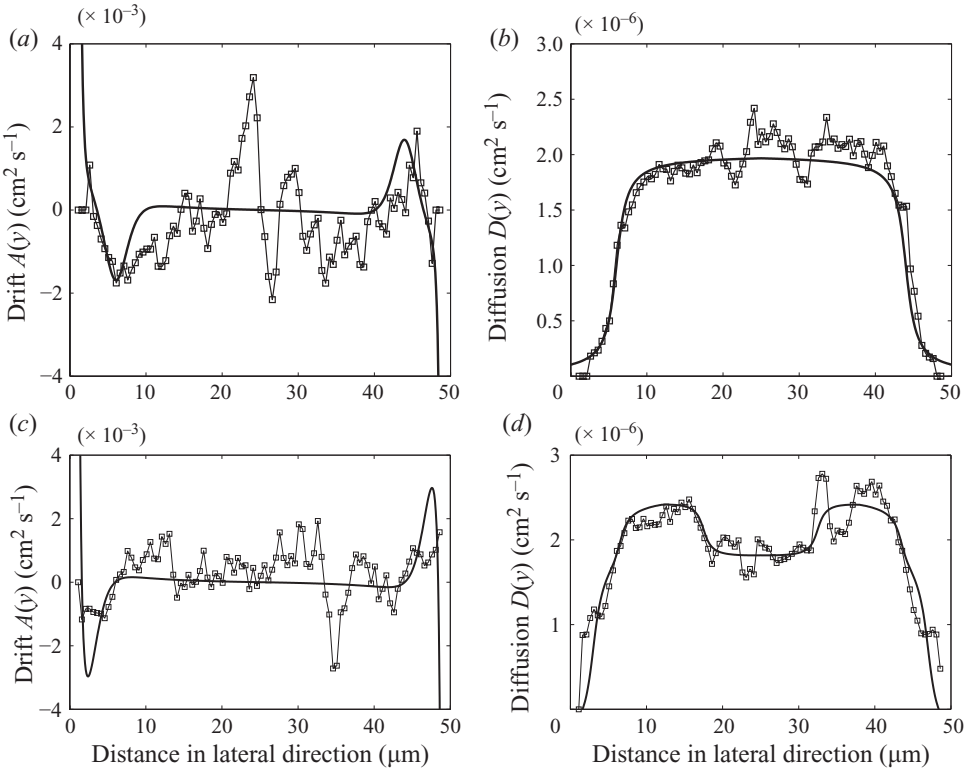

FIGURE 23. The smooth solid lines show input drift (a, c) and diffusion (b, d) in an updated drift–diffusion model for a 20 % (a, b) and 40 % (c, d) suspension with a wall shear rate of $1100\,\mathrm{s}^{-1}$. The diffusion is given by (A 1) and the drift by (A 3) with $A_m = 0.002$, $A_p = 19$ (a, b) and $A_m = 0.004$, $A_p = 23$ (c, d). The curves with markers show the reconstructed drift and diffusion functions.

In order to recover the concentration profile seen in our whole blood simulations and on the same time scale as in those simulations, we add an additional localized drift term that is motivated by our RBC orientation angle argument and is shown in figure 23. The magnitude and lateral location of the additional drift depends on haematocrit since it is assumed that this drift increases linearly with the number of RBCs and occurs adjacent to the cell-free layer. These additional drift terms are small enough to be undetectable by our drift estimation calculation in § 3.4. To show this,

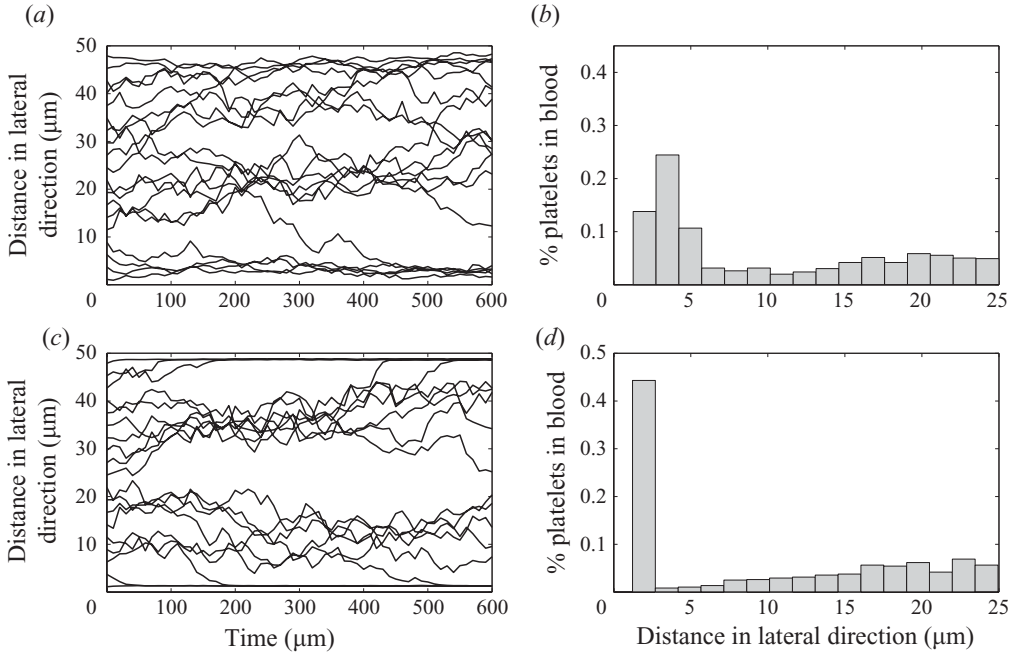

FIGURE 24. Plots of sample SDE trajectories and histograms of SDE platelet-concentration profiles after 600 ms for the shear rate $1100\,s^{-1}$ for 20 % (a, b) and 40 % (c, d) haematocrits. The additional drift towards the wall from (A 3) is included in these calculations.

we produce platelet trajectories from the SDE model and attempt to recover the input drift function using the same procedure as in § 3.4 for the IB platelet data with the same number of lateral position data points as before. The jagged lines with square markers in figure 23 show what the estimated drift function would look like after the S-G filter smoothing. This recovered drift does not approximate the input drift well enough to distinguish the real drift from noise. However, the addition of this small drift has the ability to recreate the platelet trajectories and concentration profile as seen in our whole blood simulations on the same time scale as those simulations for both 20 % and 40 % cases (see figure 24).

4. Discussion

In this paper, we perform a series of numerical experiments using a lattice Boltzmann IB method to model whole blood flow dynamics. The purpose of this work is to study a phenomenon known as lateral platelet motion and to better understand the physical mechanisms that create the platelet near-wall excess seen experimentally. In this model, RBCs and platelets are treated as IB objects with internal density and viscosity identical to that of the surrounding plasma. The fluid domain is a periodic, two-dimensional 50 μm wide channel, and the flow is driven by a constant pressure gradient.

Computational experiments in which lateral platelet motion is isolated from radially inward RBC migration are preformed by initializing simulations with pre-equilibrated RBCs and platelets uniformly distributed in the lateral direction. From these studies, we infer that lateral platelet motion does not result from the radially inward motion of RBCs. The inward motion of the RBCs may impede the motion of platelets towards the channel walls or the initial lack of an RBC-free layer may cause a lag in

lateral platelet motion. In our numerical experiments, most of the radially outward platelet motion occurs after the cell-free layer has fully developed and platelets tend to migrate into regions with more available space. The platelet near-wall excess lies in the RBC-free layer for both 20 % and 40 % haematocrit numerical experiments, and this leads us to examine the effect of excluded volume on platelet distributions. We find that platelet distributions recovered from our computational model can be largely explained by volume exclusion due to RBCs, provided that the non-zero radii of platelets are accounted for. However, this theory does not explain the presence of a dip in platelet concentration between the near-wall region and the vessel centre.

In order for platelets to redistribute uniformly in available space on the time scales examined in this paper, their random motion must be orders of magnitude greater than that of Brownian diffusion. In this study, we estimate the effective platelet diffusion at the centre of the vessel to be of the order of $10^{-6}\,\mathrm{cm}^2\,\mathrm{s}^{-1}$. The high diffusivity of platelets is due to enhanced RBC mixing in the central region of the channel. This motion gives platelets the ability to redistribute themselves quickly into the RBC-free layer, where there is more available space and platelet diffusion is relatively small. While we use the word 'diffusion' to describe this motion of the platelets, we emphasize that this word is used by analogy only. The platelet motion is driven by the complex motion of the RBCs, not by thermal forces. We also want to emphasize that while the 'diffusion' leads to a situation in which there is a higher platelet concentration near the wall when concentration is measured as a number of platelets per volume of blood, if the platelet concentration is measured as a number of platelets per volume of plasma accessible to platelets, the 'diffusion' actually functions to homogenize the platelet concentration.

This study also explores the relationship between lateral platelet motion and wall shear rate by comparing numerical simulations at shear rates of $400\,\mathrm{s}^{-1}$ and $1100\,\mathrm{s}^{-1}$. When exposed to high shear rate conditions, we find that lateral platelet motion occurs on a much faster time scale. In our numerical simulations, platelets circulate within a periodic domain between 10 and 60 times during a 600 ms simulation, depending on lateral position. In the experiments with which we compare our numerical simulations, platelets travel down capillary tubes and the platelet distribution is determined at a specific longitudinal distance from the flow chamber entrance. In order to better compare our numerical simulations to experimental observations, we estimate the platelet distribution at equal distances along the channel for different flow speeds. We accomplish this by first calculating the average flow velocity at both wall shear rates, then using it to translate simulation time to an effective axial distance. We compare the platelet distributions for both high and low wall shear rates at approximately the same axial 'distance' down the channel. It is clear that after the same amount of time, the near-wall excess of platelets at the high wall shear rate is much larger than the low wall shear rate, but when the distance down the tube instead of migration time is taken into account, the relationship is less clear. It is possible that the rate of platelet transport to the near-wall region is proportional to the wall shear rate, but for us to determine this requires running additional simulations for a wider range of shear rates. In addition to comparing the platelet-concentration profiles for different wall shear rates, we also investigate how the platelet radial diffusion is affected by the wall shear rate. When the pressure gradient driving the flow is three times larger (and hence the wall shear rate is also approximately tripled), the magnitude of the diffusion coefficient at the centre of the channel appears to increase by a similar factor.

This investigation has led to the discovery that the effective platelet lateral diffusion coefficient varies sharply in the radial direction. To our knowledge, this has not been

observed before. After estimating platelet diffusion from our whole blood simulations, we use the recovered diffusion function to simulate platelet motion using SDEs. These SDE simulations allow us to predict the effect that variable diffusion has on the temporal development of the platelet-concentration profile. Our study suggests that this variable diffusivity alone is not enough to account for the high near-wall excess found numerically in this paper and experimentally by Tilles & Eckstein (1987) and Eckstein *et al.* (1988). We then propose a possible additional drift mechanism in the form of an RBC barrier at the transition into the cell-free layer. We believe that the orientation angle that RBCs exhibit under shear-flow conditions may bias platelet motion during RBC collisions with platelets. Further evidence for this net radially outward force is the presence of a dip adjacent to the cell-free layer in the profile of platelet concentration in the available space. Volume exclusion and high diffusion alone do not predict a dip in this region of the domain.

The simulations discussed in this paper were motivated by the experimental data from Eckstein's *in vitro* experiments which were done under constant flow conditions, and so we assumed that the pressure gradient driving the flow is constant in time. The situation in arterioles *in vivo* is different in a number of ways that might impact the results we present. One difference is that arteriolar flow is pulsatile, and so the magnitude of the shear rate (and shear stress) in the arteriolar blood varies over the cardiac cycle, a typical duration of which is 750 ms to 1 s, which is a time period a little longer than that (500–600 ms) on which the phenomena of interest occur in our simulations. Another difference is that as blood enters an arteriole from a larger vessel, the RBC and platelet distributions may already be non-uniform. There are also differences between the simple tube walls we modelled here and the walls of arterioles which are lined by glycocalyx-bearing endothelial cells.

A potentially large limitation of the current studies is that they were carried out in two dimensions. In fact, at the start of this project, we were not certain whether a near-wall excess would develop in two-dimensional simulations. That it does, and that the magnitude of the near-wall excess behaves in a way seen experimentally in terms of its dependence on haematocrit and shear rate is encouraging. Still, the limitation to two dimensions may affect some of the quantitative predictions, e.g. the time scale on which the near-wall excess develops. Two particular areas of concern in making the reduction to two dimensions are treatment of the RBC membrane mechanics, and restrictions on the types of motions the RBCs and platelets may make. We hope to remove these limitations in future work, but for now, the size of a three-dimensional simulation, the need to simulate seconds of real time and the need to a sufficient number of simulations to extract useful statistics make this infeasible.

Although the grid spacing (0.14 μm) used for the simulations reported in this paper is small, it is not sufficiently small to allow us to resolve fully lubrication forces between closely apposed RBCs. However, the convergence results presented in Appendix B provide strong evidence that it does a reasonable job in capturing interactions between nearby RBCs. Furthermore, in our IB-based calculations, it is not necessary, as is in many particle methods (Pan *et al.* 2002; Climent & Maxey 2003; Vikhansky 2003); it is necessary to add a repulsive force between the particles to prevent them from overlapping. In our IB-based calculations, this is not necessary. The reason is that, in the discrete form of (2.5), an approximation to the delta function is used and, since it has support over a $4h$ by $4h$ region of the lattice, the velocity at an IB point is a weighted average of lattice velocities over this region. Hence, when two IB points on different RBCs are less than a distance $4h$ apart, there is an overlap in the lattice velocities averaged to find the IB points' respective velocities,

and the overlap becomes greater and the two IB velocities become more similar the closer the two points approach one another. In effect, because of the smeared nature of the approximate delta-function, there is a numerical lubrication force that makes it progressively harder to push two IB surfaces together the closer they are to one another. The same smearing, along with the high deformability of the RBCs in our simulations, precludes direct application of the lubrication corrections introduced by Nguyen & Ladd (2002) for rigid particles with sharp-defined boundaries.

Keeping the limitations just discussed in mind, we still think that both our simulations and the drift and diffusion extracted from them may be used to give insight into the blood clotting process. The drift–diffusion model could be used to simulate platelet motion in models of clot development without explicitly including RBCs (see Fogelson, Kuharsky & Yu 2003; Fogelson & Guy 2008). Our observation about the magnitude of the near-wall excess at different shear rates may shed light on the well-known result that platelets comprise a much lower fraction of venous clots than they do of arterial clots. Due to the much lower shear rates in the venous circulation, platelets may simply not be in a position near the wall to participate as much in clot formation.

This work was supported by NSF grants RTG DMS-0354259, VIGRE DMS-0602219, and DMS-0540779, NIGMS grant R01-GM090203 and partially supported by NIH-NCRR grant 1S10RR17214. A grant of computer time from the Center for High Performance Computing is gratefully acknowledged. The authors would also like to thank James Keener, Mike Kirby, Bob Guy and Sam Isaacson for helpful discussions.

Appendix A. Drift and diffusion equations

The smooth functions we choose for diffusion at 20 % and 40 % haematocrit flowing blood suspensions at a wall shear rate are given by

$$D_{20}(y) = \left(\frac{1}{\pi}\tan^{-1}(19 - |25 - y|) + \frac{1}{2}\right)(D_H - D_L) + D_L \tag{A 1}$$

$$\begin{aligned} D_{40}(y) = {} & \left(\frac{1}{\pi}\tan^{-1}(22 - |25 - y|) + \frac{1}{2}\right)(D_H - D_L) + D_L \\ & + \left(\frac{1}{\pi}\tan^{-1}(6.6 - 1.2 \times |12 - y|) + \frac{1}{2}\right) 2D_H/5 \\ & + \left(\frac{1}{\pi}\tan^{-1}(6.6 - 1.2 \times |38 - y|) + \frac{1}{2}\right) 2D_H/5, \end{aligned} \tag{A 2}$$

where D_H is the maximum diffusion at the centre of the vessel and $D_L = -1 \times 10^{-9}$ is chosen such that platelets away from RBCs only experience Brownian diffusion. The function for the drift is

$$A(y) = A_{WR}(y) - \text{sign}(25 - y) \times A_m \text{sech}^2(0.5(|25 - y| - A_P)), \tag{A 3}$$

where A_{WR} is the wall-repulsion drift, A_m is the magnitude of the RBC-induced drift, which is proportional to the number of RBCs in the domain, and A_p is the lateral position of this additional drift which depends on the location of the cell-free layer.

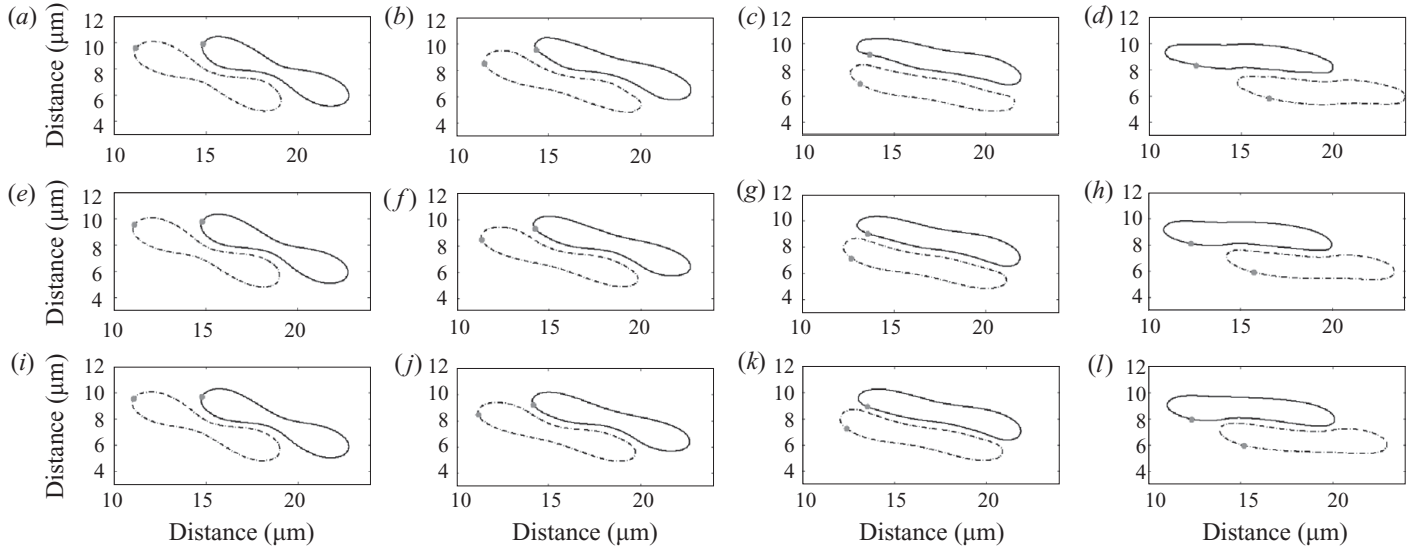

FIGURE 25. Sequence of snapshots of RBCs interacting in a shear flow. The timestep and spacestep for these simulations are (*a–d*) $2\Delta t$ and $2h$, (*e–h*) Δt and h, (*i–l*) $\Delta t/2$ and $h/2$, where Δt and h are the values used in the other simulations in this paper.

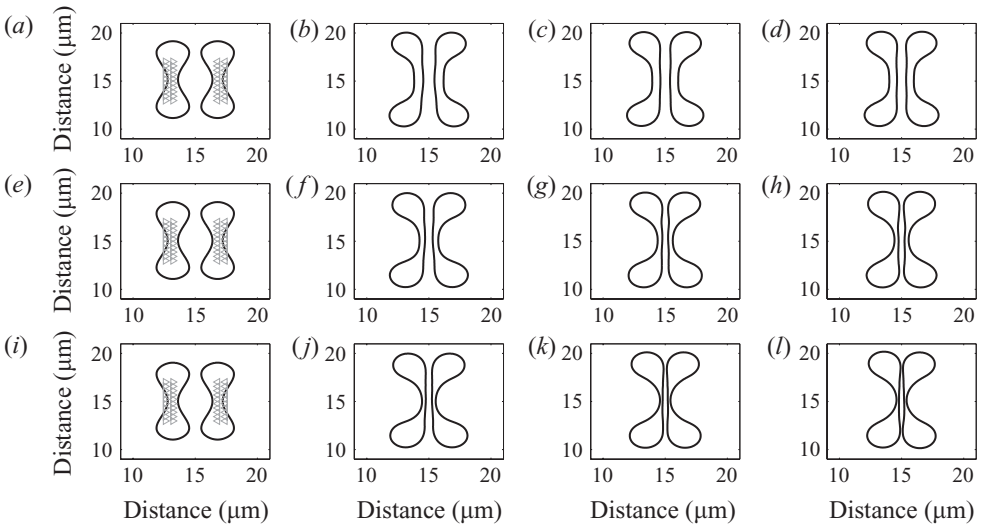

FIGURE 26. Sequence of snapshots of RBCs colliding due to external IB forces (locations shown by gray arrows). The timestep and spacestep for these simulations are (*a–d*) $2\Delta t$ and $2h$, (*e–h*) Δt and h, (*i–l*) $\Delta t/2$ and $h/2$, where Δt and h are the values used in the other simulations in this paper.

We let A_{WR}, the drift due to wall repulsion, be

$$A_{WR}(y) = \text{sign}(y_c)(5 \times 10^{-5}) \left[\exp(-4(22.8 - y_c)) - \frac{1}{400} \left(\frac{1}{25.1 - y_c} - \frac{1}{25.1} \right) \right] \quad \text{(A 4)}$$

where $y_c = |25 - y|$.

Appendix B. Numerical convergence study of interactions between a pair of nearby red blood cells

The fluid dynamics of the whole blood model presented in this paper are highly dependent on the interactions between RBCs in the flow. We have tested the accuracy of our LB-IBM approach with a convergence study of isolated RBC interactions. The results shown in the paper are for a grid spacing of $h = 1/7\,\mu\text{m}$ and time step of $\text{d}t = 2 \times 10^{-8}\,\text{s}$. Here, we compare simulations with this discretization to those on a coarser mesh with $2h$ and $2\,\text{d}t$ and on a finer mesh with $h/2$ and $\text{d}t/2$.

Figure 25 shows a series of snapshots for two RBCs exposed to a simple shear flow. These simulations demonstrate very similar time progressions for all three meshes (the mesh for the centre panels matches that of our whole blood simulations). There is a noticeable difference between the top and middle panels, both in terms of how closely the cells approach one another and in how rapidly they move pass each other. The differences between the middle and bottom panels are much smaller, which indicates that, for this interaction, the mesh used in our whole blood simulations provides an accurate solution.

For the experiment shown in figure 26, equal and opposite horizontal forces were applied to effectively drive the RBCs together. There are two sets of special IB points (shown by grey arrows in figure 26), one can be thought of as associated with each RBC. For the ones on the left, a constant (in time) force to the right was calculated

and spread to the grid like any other IB force. For the ones on the right, the equal and opposite forces were spread to the grid as well. Again, we see that the mesh spacing does not have a large effect on the behaviour and shape of the RBCs, but that it does affect how closely the cells are able to approach one another. The closest apposition between points on the two cells is approximately two mesh widths on the coarse and middle grids, and slightly more than two mesh widths on the finest grid. The physical separation between the cell surfaces at the end of the middle and finest grid calculations is approximately the same (at the same physical time) and this suggests that the 'lubrication forces' within the gap between the cells balance the applied forces.

REFERENCES

Bagchi, P. 2007 Mesoscale simulation of blood flow in small vessels. *Biophys. J.* **92**, 1858–1877.

Barthes-Biesel, D., Diaz, A. & Dhenin, E. 2002 Effect of constitutive laws for two-dimensional membranes on flow-induced capsule deformation. *J. Fluid Mech.* **460**, 211–222.

Chan, P. C.-H. & Leal, L. G. 1979 The motion of a deformable drop in a second-order fluid. *J. Fluid Mech.* **92**, 131–170.

Climent, E. & Maxey, M. R. 2003 Numerical simulations of random suspensions at finite Reynolds numbers. *Intl J. Multiphase Flow* **29** (4), 579–601.

Crowl, L. & Fogelson, A. L. 2010 Computational model of whole blood exhibiting lateral platelet motion induced by red blood cells. *Intl J. Numer. Meth. Biomed. Engng* **26** (3–4), 471–487.

Dupin, M. M., Halliday, I., Care, C. M., Alboul, L. & Munn, L. L. 2007 Modeling the flow of dense suspensions of deformable particles in three dimensions. *Phys. Rev.* E **75**, 066707-1-17.

Eckstein, E. C. & Belgacem, F. 1991 Model of platelet transport in flowing blood with drift and diffusion terms. *Biophys. J.* **60**, 53–69.

Eckstein, E. C., Tilles, A. W. & Millero, F. J. III 1988 Conditions for the occurrence of large near-wall excesses of small particles during blood flow. *Microvasc. Res.* **36**, 31–39.

Eggleton, C. D. & Popel, A. S. 1998 Large deformation of red blood cell ghosts in a simple shear flow. *Phys. Fluids* **10** (8), 1834–1845.

Fischer, T. M., Stohr-Lissen, M. & Schmid-Schonbein, H. 1978 The red cell as a fluid droplet: tank tread-like motion of the human erythrocyte membrane in shear flow. *Science* **202**, 894–896.

Fogelson, A. L. & Guy, R. D. 2008 Immersed-boundary-type models of intravascular platelet aggregation. *Comput. Meth. Appl. Mech. Engng* **197**, 2087–2104.

Fogelson, A., Kuharsky, A. & Yu, H. 2003 Computational modeling of blood clotting: coagulation and three-dimensional platelet aggregation. In *Polymer and Cell Dynamics: Multicsale Modeling and Numerical Simulations* (ed. W. Alt, M. Chaplain, M. Griebel & J. Lenz), pp. 145–154. Birkhaeuser-Verlag.

Gardiner, C. W. 2004 *Handbook of Stochastic Method for Physics, Chemistry, and the Natural Sciences*. Springer.

Goldman, A. J., Cox, R. G. & Brenner, H. 1967 Slow viscous motion of a sphere parallel to a plane wall. Part II. Couette flow. *Chem. Engng Sci.* **22**, 653–660.

Goldsmith, H. 1971 Red cell motions and wall interactions in tube flow. *Fed. Proc.* **30** (5), 1578–1588.

Goldsmith, H. L. & Marlow, J. 1972 Flow behavior of erythrocytes. Part I. Rotation and deformation in dilute suspensions. *Proc. R. Soc. Lond.* B **182** (1068), 351–384.

Guo, Z., Zheng, C. & Shi, B. 2002 Discrete lattice effects on the forcing term in the lattice Boltzmann method. *Phys. Rev.* E **65**, 1–6.

He, X., Zou, Q., Luo, L. & Dembo, M. 1997 Analytic solutions of simple flows and analysis of nonslip boundary conditions for the lattice Boltzmann [BGK] model. *J. Stat. Phys.* **87** (1/2), 115–136.

Hu, H. H. & Joseph, D. D. 1999 Lift on a sphere near a plane wall in a second order fluid. *J. Non-Newtonian Fluid Mech.* **88**, 173–184.

Koleski, J. F. & Eckstein, E. C. 1991 Near wall concentration profiles of 1.0 and 2.5 μm beads during flow of blood suspensions. *Trans. Am. Soc. Artif. Intern. Organs* **37**, 9–12.

Ladd, A. & Verberg, R. 2001 Lattice-Boltzmann simulations of particle-fluid suspensions. *J. Stat. Phys.* **104** (5/6), 1191–1251.

MacMeccan, R. M., Clausen, J. R., Neitzel, G. P. & Aidun, C. K. 2009 Simulating deformable particle suspensions using a coupled lattice-boltzmann and finite-element method. *J. Fluid Mech.* **618**, 13–39.

McLaughlin, J. B. 1993 The lift on a small sphere in wall-bounded linear shear flows. *J. Fluid Mech.* **246**, 249–265.

Nguyen, N. Q. & Ladd, A. J. C. 2002 Lubrication corrections for lattice-Boltzmann simulations. *Phys. Rev.* E **66** (4), 046708[1–12].

Pan, T. W., Joseph, D. D., Bai, R., Glowinski, R. & Sarin, V. 2002 Fluidization of 1204 spheres: Simulation and experiment. *J. Fluid Mech.* **451**, 169–191.

Peskin, C. 2002 The Immersed Boundary method. *Acta Numerica* **11**, 1–39.

Pozrikidis, C. 2001 Effect of membrane bending stiffness on the deformation of capsules in simple shear flow. *J. Fluid Mech.* **440**, 269–291.

Qian, H., Sheetz, M. P. & Elson, E. L. 1991 Single particle tracking: Analysis of diffusion and flow in two-dimensional systems. *Biophys. J.* **60**, 910–921.

Savitzky, A. & Golay, M. J. E. 1964 Smoothing and differentiation of data by simplified least squares procedures. *Anal. Chem.* **36**, 1627–1639.

Skalak, R., Tozeren, A., Zarda, R. & Chein, S. 1973 Strain energy function of red blood cell membranes. *Biophys. J.* **13** (3), 245–264.

Sui, Y., Chew, Y. T. & Low, H. T. 2007 A lattice Boltzmann study on the large deformation of red blood cells in shear flow. *Intl J. Mod. Phys.* C **18** (6), 993–1011.

Tangelder, G. J., Teirlinck, H. C. & Slaaf, D. W., Reneman, R. S. 1985 Distribution of blood platelets flowing in arterioles. *Am. J. Physiol. Heart Circ.* **248** (3), H318–H323.

Tilles, A. W. & Eckstein, E. C. 1987 The near-wall excess of platelet-sized particles in blood flow: Its dependence on hematocrit and wall shear rate. *Microvasc. Res.* **33**, 211–223.

Turitto, V. T., Benis, A. M. & Leonard, E. F. 1972 Platelet diffusion in flowing blood. *Ind. Engng Chem. Fundamen.* **11** (2), 216–223.

Vikhansky, A. 2003 A new modification of the immersed boundary method for fluid-solid flows: moderate Reynolds numbers. *J. Comput. Phys.* **191**, 328–339.

Wohl, P. R. & Rubinow, S. L. 1974 The transverse force on a drop in an unbounded parabolix flow. *J. Fluid Mech.* **62**, 185–207.

Woldhuis, B., Tangelder, G. J., Slaaf, D. W. & Reneman, R. S. 1992 Concentration profile of blood platelets differs in arterioles and venules. *Am. J. Physiol. Heart Circ.* **262** (4), H1217–H1223.

Yeh, C., Calvez, A. C. & Eckstein, E. C. 1994 An estimated shape function for drift in a platelet-transport model. *Biophys. J.* **67**, 1706–1716.